Ultrasonic evaluation of self-healing cementitious materials with superabsorbent polymers: Mortar vs. concrete

Lefever, Gerlinde; Charkieh, Ahmad Shawki; Abbas, Mustafa; Van Hemelrijck, Danny; Snoeck, Didier; Angelis, Dimitrios

Published in:
Developments in the built environment

DOI:
10.1016/j.dibe.2022.100112

Publication date:
2023

Developments in the Built Environment 13 (2023) 100112

Contents lists available at ScienceDirect

Developments in the Built Environment

journal homepage: www.sciencedirect.com/journal/developments-in-the-built-environment

Ultrasonic evaluation of self-healing cementitious materials with superabsorbent polymers: Mortar vs. concrete

Gerlinde Lefever [a,*], Ahmad Shawki Charkieh [a], Mustafa Abbass [a], Danny Van Hemelrijck [a], Didier Snoeck [a,b], Dimitrios G. Aggelis [a]

[a] Department Mechanics of Materials and Constructions, Vrije Universiteit Brussel (VUB), Pleinlaan 2, 1050, Brussels, Belgium
[b] BATir Department, Université Libre de Bruxelles (ULB), 50 F.D. Roosevelt Avenue, 1050, Brussels, Belgium

ARTICLE INFO

Keywords:
Cement
Self-healing
Ultrasound
Superabsorbent polymers (SAPs)
Hydrogel

ABSTRACT

The inclusion of superabsorbent polymers (SAPs) has become increasingly attractive to promote the self-healing ability of cementitious materials, thereby reducing the costs related to manual repairs. To advocate the use of these additives within large-scale constructions, an assessment of the self-healing ability is needed to ensure the safety of infrastructures. A non-destructive evaluation method was found in the adoption of ultrasonic monitoring. Thanks to the sensitivity of ultrasound to the elastic properties, the technique allows to determine the self-healing effectiveness and to compare the healing capacity between different mixtures. However, most studies concerning ultrasonic assessments of the healing evolution were conducted on mortars, lacking large aggregates. Therefore, to upgrade to the most commonly used construction material, self-healing of concrete is monitored, and its performance is compared to mortar. Ultrasonic surface wave monitoring shows the potential to evaluate the crack closure in either mixture and the effect of different SAPs included.

1. Introduction

Concrete is known as a robust construction material. However, when tensile stresses are generated, the material is susceptible to cracking. As these cracks provide a passageway for deleterious liquids to enter deeper matrix layers, affecting the durability and eventually the mechanical performance, the adequate repair of cracks became a point of concern. While manual repairs come with high costs and labour, self-healing cementitious materials are characterized by an automatically activated repair process upon crack creation and provide a solution in case of limited accessibility. Cementitious composites show the capacity to seal and heal cracks through autogenous healing, which is mainly induced by the continued hydration of unhydrated cement particles and the precipitation of $CaCO_3$ (Van Tittelboom and De Belie, 2013) (Hossain et al., 2022). While these mechanisms occur simultaneously, the further hydration of cement particles only lasts until all unhydrated cement is consumed. The dissolution and carbonation of calcium hydroxide continues for a longer period (Snoeck and De Belie, 2019). Essential for the initiation of these processes, and thus for autogenous healing, is the availability of water inside the cracks. To maintain the humidity within the cracks, superabsorbent polymers (SAPs) have been studied extensively in literature (Snoeck et al., 2014) (Lefever et al., 2020a) (Kanellopoulou et al., 2021) (Schröfl et al., 2022). Thanks to their high absorption capacity, SAPs absorb water from the environment and generate water-filled reservoirs inside the cracks. In this way, they physically block the crack entrance, leading to self-sealing. Afterwards, the water is released and enhances the autogenous healing process. It should be mentioned that, despite their benefit for the promotion of self-healing, the addition of SAPs increases the macro porosity, which negatively affects the mechanical performance (Craeye et al., 2011) (Wehbe and Ghahremaninezhad, 2017). Care should thus be taken on the amount of SAPs that is included in cementitious mixtures.

Whereas SAPs clearly show the potential to improve the self-healing ability, the assessment of the healing effectiveness is of utmost importance, both from a material's point of view, i.e. to optimize the mixture design, as to ensure the safety of structures in use. On the lab-scale, diverse evaluation methods have been used to determine the self-healing effectiveness. Most prominent are microscopic analysis (Suleiman et al., 2019), water permeability (Wang et al., 2014) (Van Mullem et al., 2019) and mechanical tests (Qian et al., 2009) (Snoeck and De Belie, 2015). While the former two methods only evaluate the "sealing" ability of a cementitious mix, and thus not the actual healing capacity,

* Corresponding author.
E-mail address: Gerlinde.Lefever@vub.be (G. Lefever).

https://doi.org/10.1016/j.dibe.2022.100112
Received 30 September 2022; Received in revised form 13 December 2022; Accepted 13 December 2022
Available online 14 December 2022

mechanical tests allow to directly assess the regain in mechanical performance. However, due to their destructive nature, these tests cannot be applied for in-situ applications and a follow-up of the healing progress on the same specimen remains impractical. For this reason, recent research has focused on the adoption of non-destructive testing methodologies to assess the healing ability. A solution was found using ultrasound, due to the sensitivity of ultrasonic waves to the elastic properties of the material under study. The medium they travel through defines the travelling speed and changes the waveform shape in a way that is characteristic of its microstructure. Ultrasound has been used for the characterization of many different materials. Specific for cementitious mixtures, ultrasound has been used to determine the setting time (De Belie et al., 2005) (Lefever et al., 2020b), to estimate the mechanical performance (Kaplan, 1959) (Popovics, 2001) (Haach et al., 2015), to identify voids or damage (Chaix et al., 2006) (Selleck et al., 1998) (Antonaci et al., 2010) and, more recently, to monitor the healing evolution (Aggelis et al., 2009) (Ahn et al., 2017) (Tsangouri et al., 2019) (Lefever et al., 2020c) (Ahn et al., 2021). The previous studies describe the use of surface wave measurements, where emitter and receiver(s) are placed on a single surface of the specimen under study. The adoption of ultrasound showed to be able to distinguish between the uncracked and cracked state through an analysis of various wave parameters. Specifically, upon cracking, the longitudinal wave velocity decreased as the travel path became longer due to the created discontinuity. Also, the amplitude of the signal decreased, as a large portion of the wave energy gets scattered onto the crack walls. Upon the deposition of healing products within the crack, these wave parameters increased again, thereby suggesting the closure of cracks. A confirmation with the visual crack closure, determined by microscopic analysis, was established.

Ultrasonic self-healing evaluation has clearly shown its potential in previous studies. As mainly mortar mixtures were investigated, it would be interesting to expand the literature towards concrete mixtures and compare the effectiveness of SAPs on the healing process between mortars and concrete. Although both materials share common matrix characteristics, the existence of large aggregates in high volume content within concrete complicates the conditions, as they pose large discontinuities in the cement matrix. In addition, another question that arises is whether ultrasound can discriminate between the healing potential of different SAPs, paving the way for a mixture optimization process through ultrasonic assessment. Therefore, in this study, mortar and concrete blends with and without different superabsorbent polymers were investigated. At first, the intact microstructure was evaluated through ultrasonic measurements. Secondly, the specimens were cracked and the healing process within these specimens was monitored during wet-dry curing, to promote the occurrence of a self-healing mechanism. At the same time, microscopic measurements of the crack width were performed to validate the ultrasonic results at the surface. The results revealed a clear correlation between the ultrasonic measurements and the microscopic analysis. While the exact mechanisms behind autogenous healing in mortar and concrete are still under consideration, the outcome of this study supports the use of ultrasonic measurements for the assessment of the self-healing effectiveness.

2. Materials and methods

2.1. Materials

Four mortar compositions and their equivalent concrete blends were investigated. The first is a reference mixture without additives, while the three other contain superabsorbent polymers. For all compositions, Portland cement CEM I 52.5 N Strong from Holcim (Belgium) was used. As fine aggregates, river sand 0/2 was added in an amount of 2 to 1 with respect to the weight of the cement for mortar and in a weight amount of 1.27 to 1 for concrete. Concerning the concrete specimens, medium and large aggregates were added in an amount of 1.27 to 1 and 2.36 to 1, respectively. The medium-sized aggregates consist of rounded grains with a diameter between 4 mm and 8 mm, while the larger gravel particles have a size between 6.3 mm and 14 mm. The water-to-cement ratio was maintained for all mixtures and was equal to 0.35. As this ratio is relatively low, a superplasticizer was added to increase the workability. The superplasticizer used was MasterGlenium 51 (conc. 35%) from BASF and was added in an amount of 0.4% and 0.6% with respect to the weight of cement, for mortar and concrete, respectively.

Three types of superabsorbent polymers were used, being Floset27 CS and Floset27 MB from SNF (France) and VP400 from BASF (Germany). Both former SAPs have an identical chemical composition: they are cross-linked copolymers of acrylamide and acrylic acid. The particle sizes are however different, being between 0 and 300 μm for Floset27 CS, with a mean particle diameter of 190 μm, and between 0 μm and 1000 μm for Floset27 MB. An intermediate size of this superabsorbent was already studied in literature and showed an improved healing ability within cementitious mixtures (Gruyaert et al., 2016) (Pelto et al., 2017). The third type of superabsorbent polymer (VP400) used is a copolymer of acrylamide and sodium acrylate, being similar to the composition of the Floset27 series. The particle size distribution can be summarized as following: $d_{10} = 25$ μm, $d_{50} = 70$ μm and $d_{90} = 140$ μm. Whereas the Floset27 CS and VP400 polymers have relatively small sizes, and are therefore more suitable for internal curing purpose (De Meyst et al., 2021) (Lefever et al., 2021), VP400 has proven its effectiveness for the promotion of autogenous healing in previous studies as well (Lefever et al., 2020a) (Snoeck and De Belie, 2015). The amount of SAPs included was fixed at 0.5% by weight of the cement. Additional water was added to the mixtures with SAPs to take account of their water uptake. By means of a flow table test, following NBN EN 1015-3 (Belgisch instituut voor normalisatie (BIN), 1999), an identical workability of the reference and SAP mortars was obtained for additional amounts of 20 g, 25 g and 30 g of water per gram of SAP, for Floset27 CS, Floset27 MB and VP400, respectively. These same amounts were then also added to the concrete blends. It should be mentioned that the SAPs were added to the mixing bowl in the dry state to ensure proper dispersion of the particles prior to adding the total water with the dissolved superplasticizer.

2.2. Sample preparation

For every mixture composition, four prism specimens were cast. The mortar samples measured 40 mm × 40 mm x 160 mm, while the concrete beams have dimensions of 100 mm × 100 mm x 400 mm. After one day of curing, the specimens were demoulded and cured in plastic foil for 28 days at a temperature of 20 ± 2 °C. To assess the self-healing ability, it was chosen to create a single crack within each specimen, having an average width of 150 μm. To keep the cracked specimens together and control the crack width, a unidirectional carbon fibre reinforced polymer (CFRP) laminate, PC® CARBOCOMP UNI from TRADECC, was glued on top of the mortar and concrete specimens by means of an epoxy resin. An example for a concrete specimen is shown in Fig. 1 (a). The CFRP strip was glued two days before cracking, to allow for the hardening of the epoxy resin. After 28 days of curing, the specimens were cracked during a three-point bending test at a speed of 0.5 mm/min, leading to a single through-going crack without separation of the two specimen halves due to the CFRP action, in order to guarantee that the SAPs would remain in position. Then, the specimens were placed inside a metal frame (see Fig. 1 (b)), which pushed the two halves together by screwing the nuts at both sides, until the crack width was measured at 150 μm with the microscope. The frameworks were then kept in place during the entire testing period.

To promote the autogenous healing mechanism, the specimens were placed in wet-dry curing cycles for 28 days after cracking. These cycles consisted of 1 h submersion in water at 20 ± 2 °C and 23 h of dry conditions at 20 ± 2 °C and 65 ± 5% RH.

(a) (b)

Fig. 1. (a) Gluing of the CFRP laminates on a concrete specimen and (b) concrete specimen inside a metal frame for restraining of the crack width.

2.3. Ultrasonic surface wave measurements

The evolution of the crack closure was monitored by means of ultrasonic surface wave measurements. For the mortar specimens, the set-up consisted in the placement of three R15α sensors (Mistras Group, Inc.) on a single specimen's surface, being one emitter and two receivers. The sensors have a resonant frequency of 150 kHz. In the uncracked state, the sensors were positioned at 35 mm to characterize the intact material. After cracking, the receivers were placed at opposite sides of the crack to obtain information on the created discontinuity, as shown in Fig. 2 (a). The emitter was positioned outside of the region of interest and was connected to a waveform generator, which sent a 5 V single cycle sine wave of 150 kHz. Concerning the concrete samples, a similar set-up was utilized, but with a distance of 40 mm between the receivers (Fig. 2 (b)). Also, the emitter was taken out and the excitation was performed through pencil lead breaking. The breaking of a thin pencil lead by a mechanical pencil generates a broadband wave signal. An example waveform and FFT of this waveform are shown in Fig. 3. For the connection of the sensors in both set-ups, a vacuum grease was utilized as a coupling agent. It should be mentioned that an absolute identical coupling between various measurements is difficult to achieve. Nonetheless, it is believed that very similar coupling conditions were obtained throughout all measurements, as the experiments were conducted by the same, trained researcher. The monitoring consisted in emitting multiple wave signals and the analysis was based on a minimum of five representative waves. The sampling rate was equal to 10 MSPS.

An analysis of two wave parameters was performed to follow up the healing progress. These parameters are the longitudinal wave velocity and the attenuation. In Fig. 4 (a), an example of two waveforms received from an ultrasonic experiment on an intact mortar and concrete specimen are shown. Following the excitation, the wave signal was captured by two receivers. 'Receiver 1' signifies the sensor closest to the excitation, while the second receiver was placed further away. Later on, after cracking, this denomination was maintained, and the crack was located in the middle of these two receivers. The arrival of the longitudinal wave can be noticed by the first deviation from the noise level, shown by the green arrows in Fig. 4. This onset time was determined mathematically as the moment at which the voltage level was 10% higher than the maximum noise received during the pre-trigger stage. Focusing on the mortar specimen, a travel time of 8.8 μs was observed between the arrival of the wave at both sensors. Taking into account the distance of 35 mm between the receivers, a longitudinal wave velocity of approximately 3977 m/s was calculated, which corresponds to a high quality matrix material (Naik et al., 2003). Concerning the concrete example, the travel time was 9.3 μs. With a distance of 40 mm between the sensors, one could find a longitudinal wave velocity of around 4301 m/s. The higher velocity compared to the mortar can be explained by the additional aggregates, which increase the stiffness of the material that is directly linked to the wave velocity results.

In Fig. 4 (b), an example of the waveforms received in the cracked state is shown. Compared to the uncracked situation, the signal received by the closest sensor has similar amplitude, while for the second receiver the amplitude has lowered significantly, due to the air gap within the travel path. Additionally, the arrival of the longitudinal wave is delayed in both mortar and concrete, leading to a velocity of approximately 2500 m/s for mortar and 2353 m/s for concrete in these specific cases.

Besides the longitudinal wave velocity, the attenuation was calculated. This parameter is based on the amplitude of the received waveforms, as measured by the voltage of the highest cycle. The attenuation is defined as the relative reduction of the amplitude, as the wave propagates through the material. Factors that increase the attenuation are the presence of voids, aggregates, cracks, the inherent damping of the material under study, as well as the wavefront spreading. Due to the interaction of the wave with these scatterers, a receiver that is placed further away captures a signal with reduced amplitude. From Fig. 4 (a), a decrease in amplitude from 4.23 V in the first sensor to 1.86 V in the second sensor was noticed for the mortar mixture. The attenuation can then be calculated by:

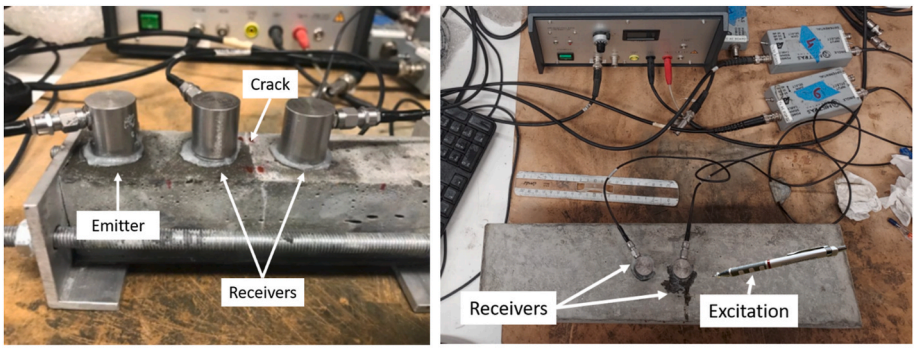

(a) (b)

Fig. 2. Ultrasonic set-up on (a) mortar and (b) concrete specimens.

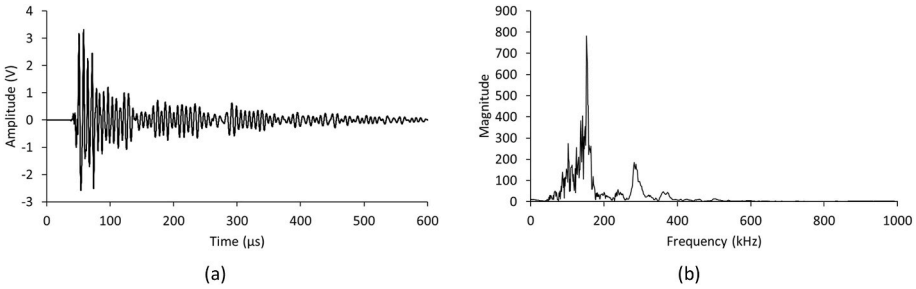

Fig. 3. (a) Waveform received after breaking of a thin pencil lead and (b) FFT of this waveform.

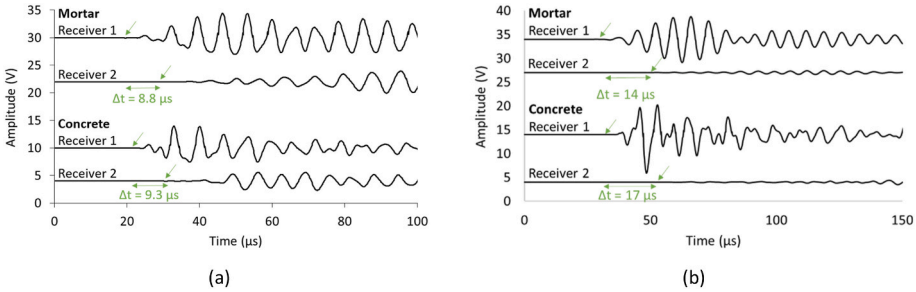

Fig. 4. Typical waveforms received from ultrasonic experiments on (a) uncracked and (b) cracked mortar and concrete specimens. The waveforms are shifted upward with respect to their original amplitude values to obtain a global view on the results.

$$Attenuation\left[\frac{dB}{mm}\right] = -\frac{1}{x}*20*log\left(\frac{A_2}{A_1}\right)$$

where A_1 and A_2 are the amplitudes in Volts of the closest and furthest sensor, respectively, and x is the distance between the sensors in mm. With the previously mentioned amplitudes, an attenuation value of approximately 0.20 dB/mm was obtained for the example case.

The calculation of the longitudinal wave velocity and attenuation was repeated at various moments within the wet-dry curing cycles. At first, the uncracked state was evaluated after 28 days of curing in plastic foil. The specimens were then cracked, and similar measurements took place immediately after cracking and after 3, 7, 14 and 28 days of curing in wet-dry cycles. As the specimen's degree of saturation varies due to the application of wet-dry curing, the ultrasonic experiments were conducted at the same moment within these cycles, i.e. 16 h after the onset of the dry period, in order to eliminate the effect of a varying water content.

2.4. Microscopic analysis

The crack width openings were measured through microscopy by means of a Leica S8 APO microscope, mounted with a DFC 295 camera. Immediately after cracking, the microscope was utilized to obtain an average crack width of 150 µm. As explained in the sample preparation section, the mortar and concrete specimens were placed inside a metal frame and the restraining was alternated with crack width measurement until the target crack size was obtained. Pictures were then taken in two locations for the mortar specimens and three locations for the concrete specimens. Per picture, five measurements of the crack width were carried out, leading to a total of 10 and 15 values per specimen, for mortar and concrete respectively. These measurements were then repeated in the exact same locations after 3, 7, 14 and 28 days in wet-dry curing cycles.

3. Results and discussion

3.1. Ultrasonic surface wave measurements

First, the evolution of the longitudinal wave velocity and the attenuation are detailed for the mortar and concrete mixtures under study. Both parameters were calculated from multiple ultrasonic experiments and an average value per measuring day was retrieved. In order to clearly reveal the observed trends, the variations on these averages are not included in the graphical representations, but are listed in Table 1. Fig. 5 (a) and (b) represent the wave velocity over time, for mortar and concrete, respectively. To facilitate the comparison between the different mixtures and increase the comprehensibility, the legends in these and all following graphs represent increasing SAP sizes from top to bottom, being VP400 (smallest), Floset27 CS (medium) and Floset27 MB (largest). Two velocity values can be distinguished per mixture series at day 0, namely one in the uncracked state and one after cracking. The intact state is characterized by the higher velocities, reaching between 3600 m/s and 4000 m/s for the mortar mixtures. The mortar containing VP400 SAPs showed a lower velocity, which could be explained by the increased porosity, as the SAPs release their absorbed water and leave behind macro pores (Wehbe and Ghahremaninezhad, 2017). On the other hand, within the Floset27 series a slight increase in wave velocity was noticed. Whereas the SAPs create macropores, the release of water from the SAPs provides internal curing to the cementitious matrix, leading to a higher amount of hydration products and a densification of the matrix (Hasholt et al., 2010). The reason why these distinct trends were noticed for VP400 vs. Floset27 specifically, lies in the large absorption capacity of the VP400 SAPs, i.e. 30 g of water per gram of SAP compared to 20 g/g and 25 g/g. For an amount of 0.5% SAP added, the mixtures with VP400 have a total W/C ratio equal to 0.5, while for Floset27 CS and Floset27 MB this is 0.45 and 0.475. After introduction of the bending crack, the velocity decreased strongly, due to the discontinuity between the two receivers. The specimens were then placed in wet-dry curing cycles and it was noticed that the velocity increased over time, demonstrating a partial restoration of the elastic properties along the travel path and therefore a filling of the crack. After 28 days of wet-dry curing, the specimens with VP400 showed the highest

Table 1
Longitudinal wave velocity (m/s) and restoration of longitudinal wave velocity after healing (%) of the mortar and concrete mixtures in the cracked, uncracked and healed stages.

		Mortar		Concrete	
		Longitudinal wave velocity (m/s)	Restoration (%)	Longitudinal wave velocity (m/s)	Restoration (%)
Reference	Uncracked	3970 ± 243	n/a	4311 ± 171	n/a
	Cracked	2505 ± 153	n/a	2296 ± 185	n/a
	3 days	2674 ± 97	13	2751 ± 85	22
	7 days	2710 ± 78	14	2730 ± 85	21
	14 days	2903 ± 297	30	2761 ± 77	18
	28 days	2973 ± 263	32	2685 ± 119	29
VP400	Uncracked	3593 ± 178	n/a	4227 ± 211	n/a
	Cracked	2275 ± 63	n/a	2115 ± 108	n/a
	3 days	2497 ± 138	17	2454 ± 29	10
	7 days	2894 ± 368	48	2625 ± 51	24
	14 days	3345 ± 359	82	2573 ± 104	22
	28 days	3322 ± 271	81	2637 ± 44	38
Floset27 CS	Uncracked	4029 ± 224	n/a	4363 ± 146	n/a
	Cracked	2601 ± 252	n/a	2274 ± 55	n/a
	3 days	2829 ± 273	11	2430 ± 62	7
	7 days	2862 ± 364	18	2944 ± 50	33
	14 days	2903 ± 383	21	3689 ± 86	71
	28 days	2886 ± 248	19	3568 ± 54	68
Floset27 MB	Uncracked	3994 ± 468	n/a	4564 ± 27	n/a
	Cracked	2482 ± 159	n/a	2664 ± 147	n/a
	3 days	2591 ± 267	3	3154 ± 89	26
	7 days	2536 ± 142	3	3289 ± 126	34
	14 days	2807 ± 158	19	3536 ± 118	53
	28 days	3094 ± 466	48	3726 ± 34	63

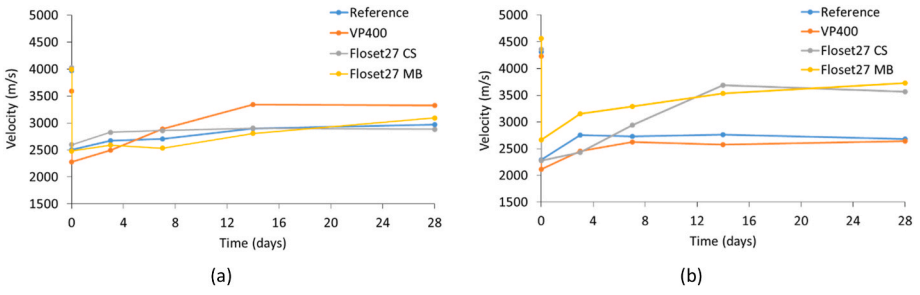

Fig. 5. Evolution of the longitudinal wave velocity vs. time for (a) mortar and (b) concrete mixtures.

restoration, while the enhancements for the Floset27 series were closely related to the reference mixture.

Fig. 5 (b) depicts the evolution of the longitudinal wave velocity for the concrete specimens. A similar trend was obtained compared to the mortar specimens, being the strong decrease in velocity upon cracking and the improvement afterwards, caused by the wet-dry cycles. However, the difference with the mortar blends was found in the higher restoration for both Floset27 SAPs. As the average particle size of these SAPs is larger compared to VP400, an increased healing ability is expected (Snoeck et al., 2014). Nonetheless, it should be mentioned that other SAP characteristics, like the kinetics of desorption, affect the healing ability. For instance, when the water absorbed by the SAPs is released too quickly, a notable amount of water will simply escape from the crack through leakage and evaporation, rather than to induce further hydration. Another explanation for the higher velocity of Floset27 concrete mixtures upon healing could be the higher saturation degree of concrete specimens, due to their larger dimensions. This means that the SAPs also more likely contain a higher amount of water during the ultrasonic test, thus being more swollen, which gives rise to additional contact points between the crack walls, certainly when larger SAPs are used.

To enable a more thorough comparison between the different mortar and concrete mixtures, the restoration percentage in terms of velocity was calculated. The latter parameter was defined as the increase in velocity upon wet-dry curing compared to the decrease due to cracking. In this respect, the differences in velocity values in the intact and cracked stages are considered, in order to solely compare the self-healing capacity of the various mixtures. The restoration capacity was calculated by:

$$Restoration\ [\%] = \frac{Q_{av.,healed} - Q_{av.,cracked}}{Q_{av.,uncracked} - Q_{av..,cracked}} * 100$$

where $Q_{av.,X}$ signifies the average of the parameter under study, being the longitudinal wave velocity (and later on the attenuation), at moment X. The average values per mixture type are summarized in Table 1.

When comparing the restoration percentages between the different compositions of mortar and concrete respectively, the general improvement in the self-healing capacity upon the inclusion of SAPs can be noticed. However, strong discrepancies emerge between the two material types. In mortar, the best healing performance is noted with the VP400, reaching a restoration of more than 80% in wave velocity. However, for concrete, the SAPs that perform the best are the two Floset27 types, which have a larger particle size.

Next to the longitudinal wave velocity evolution, a follow-up of the attenuation was conducted. The attenuation values are graphically represented in Fig. 6, whereas the exact values and their standard

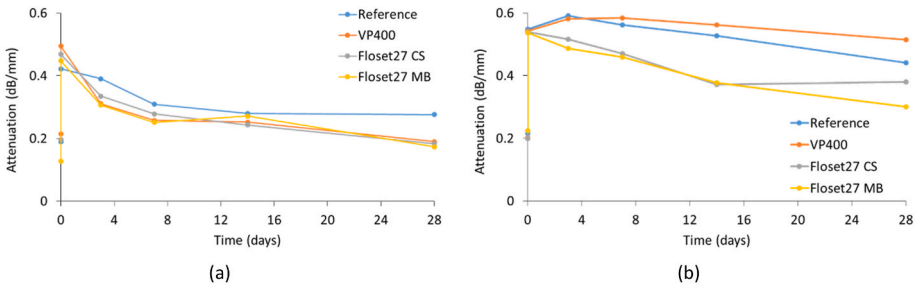

Fig. 6. Evolution of the attenuation vs. time for (a) mortar and (b) concrete mixtures.

deviation are summarized in Table 2. Focusing on the mortar mixtures in Fig. 6 (a), an opposite trend with respect to the wave velocity was seen. In the uncracked state, the attenuation values were relatively small, revealing the undamaged, dense microstructure. Upon crack creation, the attenuation increased to values between 0.40 dB/mm and 0.50 dB/mm. This increase in attenuation is caused by the fact that most of the wave energy is reflected onto the crack boundary, leading to smaller amplitude values in the second receiver. The specimens were then cured in wet-dry cycles for 28 days and a gradual reduction of the attenuation occurred. In case of the reference mortar, this decreasing trend was more noticeable within the first two weeks, while for the samples with SAPs a more continued reduction took place, indicating a continued and therefore improved healing process. After 28 days, the attenuation measured in VP400 and Floset27 CS specimens reached a smaller value compared to the intact state, implying an improvement in the material's microstructure after healing. This can be explained by the deposition of healing material within the crack. As the attenuation is sensitive to the presence of cavities/defects, which are always present within cementitious materials, the filling through healing material could improve the pathway between the sensors compared to the intact state. To confirm the improved restoration of the attenuation in SAP specimens, a representative reference and VP400 sample were broken after 28 days of wet-dry curing to visualize the internal crack volume. A picture of the crack walls can be found in Fig. 7. Focusing on the reference specimen, being the two upper halves, white zones were noticed at the left, right and

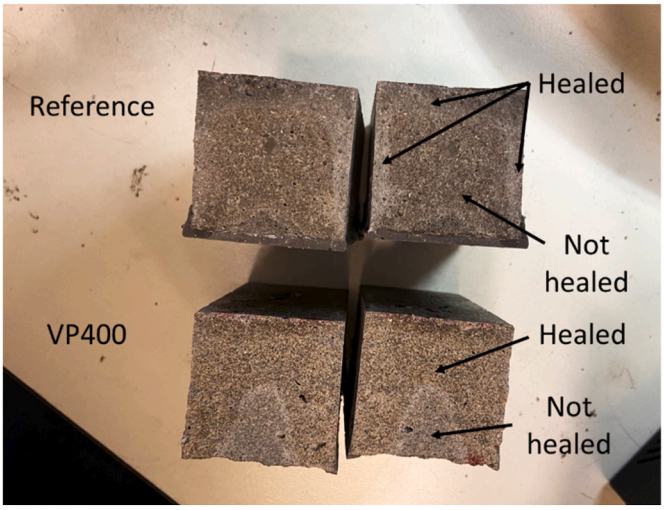

Fig. 7. Visualization of crack walls after 28 days of wet-dry curing of reference (upper halves) and VP400 (lower halves) specimens.

Table 2
Attenuation (dB/mm) and restoration of attenuation after healing (%) of the mortar and concrete mixtures in the cracked, uncracked and healed stages.

		Mortar		Concrete	
		Attenuation (dB/mm)	Restoration (%)	Attenuation (dB/mm)	Restoration (%)
Reference	Uncracked	0.19 ± 0.04	n/a	0.22 ± 0.01	n/a
	Cracked	0.42 ± 0.09	n/a	0.55 ± 0.02	n/a
	3 days	0.39 ± 0.08	6	0.59 ± 0.03	−13
	7 days	0.31 ± 0.05	45	0.56 ± 0.03	−10
	14 days	0.28 ± 0.06	56	0.53 ± 0.02	5
	28 days	0.28 ± 0.01	58	0.44 ± 0.02	29
VP400	Uncracked	0.22 ± 0.04	n/a	0.20 ± 0.01	n/a
	Cracked	0.49 ± 0.03	n/a	0.54 ± 0.03	n/a
	3 days	0.31 ± 0.04	68	0.58 ± 0.02	−17
	7 days	0.26 ± 0.05	85	0.58 ± 0.02	−26
	14 days	0.25 ± 0.04	89	0.56 ± 0.01	−16
	28 days	0.19 ± 0.03	112	0.51 ± 0.02	2
Floset27 CS	Uncracked	0.20 ± 0.03	n/a	0.20 ± 0.02	n/a
	Cracked	0.47 ± 0.03	n/a	0.54 ± 0.05	n/a
	3 days	0.34 ± 0.04	49	0.52 ± 0.01	6
	7 days	0.28 ± 0.05	70	0.47 ± 0.01	20
	14 days	0.24 ± 0.03	82	0.37 ± 0.02	34
	28 days	0.18 ± 0.01	104	0.38 ± 0.04	36
Floset27 MB	Uncracked	0.13 ± 0.03	n/a	0.22 ± 0.01	n/a
	Cracked	0.45 ± 0.02	n/a	0.54 ± 0.01	n/a
	3 days	0.31 ± 0.01	45	0.49 ± 0.02	16
	7 days	0.25 ± 0.02	61	0.46 ± 0.04	25
	14 days	0.27 ± 0.04	55	0.38 ± 0.01	39
	28 days	0.17 ± 0.05	87	0.30 ± 0.05	58

upper boundaries, as well as in few discrete spots spread over the cross-section. These white zones are an indication of the deposition of healing products. Close to the CFRP laminate, another white zone can be noticed, which can be caused by the entrapment of air upon gluing the CFRP laminates or leakage of water through the laminates. The lower halves, being a specimen with VP400, show a clear pyramidal front with varying color, of which the base lies at the CFRP laminate. The grey-like color within the triangular zone depicts the cementitious matrix. Around the pyramid, whitish crystals are deposited with a seemingly different morphology compared to the cementitious matrix. This result confirms the deposition of healing products at increasing depths on top of the surficial crack closure (see Section 3.2) and follows the trends observed in literature (Fan and Li, 2014); i.e. as water accesses the crack from the left, top and right sides, a higher deposition of healing products is expected outside of the pyramidal zone, closer to the edges.

Within the concrete samples, an analogous trend in the evolution of the attenuation parameter was observed. In Fig. 6 (b), a large increase in attenuation was obtained after cracking of the specimens, resulting in an attenuation of approximately 0.54 dB/mm for all mixtures. Within the reference and VP400 specimens, an increase of the attenuation was noticed within the first three days of wet-dry curing. This can be explained by a possible withdrawal of debris from the crack, caused by the movement of water during the healing cycles. For all cases eventually, a decrease of attenuation was measured being stronger for the Floset27 SAPs, which also provided better restoration in wave velocity as aforementioned. Specifically, the Floset27 MB mixture reached an attenuation of 0.3 dB/mm at 28 days, very close to the uncracked value. The discrepancy compared to the mortars can be noticed in the descent of the attenuation over time. The mortar mixtures show a rapid decrease within the first three days of curing, which slows down afterwards. In the case of concrete, the reduction of attenuation occurs more gradually from the start of wet-dry curing, but continues at this rate for a longer period. This can be justified by the ease of access to unhydrated cement particles and $Ca(OH)_2$ in mortar, which are then rapidly consumed. Within concrete, the crack faces show a significant amount of aggregates, being approximately 75% of the volume compared to 55% in mortar. The presence of aggregates hindering the contact between water and reactants, while at an aggregate location there is only deposition, no formation, of healing products.

Focusing on the restoration percentages of the attenuation, an improvement through the inclusion of all types of superabsorbent polymers was noticed within mortar mixtures, while in concrete only the Floset27 SAPs improved the healing capacity in comparison to the reference. While both the longitudinal wave velocity and the attenuation showed to be sensitive to the crack filling process, it is noticeable that the restoration of the attenuation is higher than the velocity restoration in mortar. This trend was also observed during numerical simulations of the healing process and signifies that the healing products present within the crack have attained a certain stiffness (Lefever et al., 2022). Concerning the concrete specimens, an opposite trend was noticed, being a higher restoration of the velocity compared to the attenuation. The reason could be that inside concrete a small amount of healing products would enable a stiff connection between aggregates on opposing crack walls, thereby restoring the longitudinal wave velocity, which is measured by the first threshold crossing that can be triggered by a small part of the "ballistic", or forward scattered wave. When focusing on attenuation, multiple scattering of the wave signal onto the aggregates still occurs, each time affecting the wave amplitude and thus lowering the observed attenuation restoration.

3.2. Microscopic analysis

Using microscopic analysis, the visual crack closure was assessed. Measurements of the crack width opening were conducted at the same moments as performing the ultrasonic experiments. For the mortar specimens, a total of 10 measurements was taken, while for the larger concrete specimens 15 crack width measurements were adopted. An example of the pictures taken during microscopic analysis of a reference mortar and the measuring procedure is visualized in Fig. 8. The measurement of the crack width is performed perpendicular to the crack's propagation path. It can be seen that during the application of wet-dry curing cycles healing products are deposited between the crack walls, thereby reducing the crack width.

Fig. 9 (a) and (b) show the average crack width per composition of mortar and concrete, respectively. The exact values and their standard deviations are listed in Table 3. Concerning the mortars, a significant difference in the crack closure between the various mixtures was seen. Immediately after cracking, the average crack width opening was approximately equal to 150 μm, as the samples were restrained to this target crack width. The placement in wet-dry curing cycles then induced a rapid partial crack closure for the reference and VP400 blends during the first three days of curing, while for the Floset27 series the reduction was only marginal. Eventually, after 28 days of healing, the best result was obtained for the VP400 mortars, yielding an average crack size of 15 μm. The minimum crack closure was obtained for the Floset27 CS specimens, i.e. leading to a crack size of about 115 μm, which was also seen upon the monitoring of the longitudinal wave velocity.

In Fig. 9 (b), the evolution of the crack opening within concrete mixtures is depicted. In case of the SAP mixtures, a higher improvement was noticed for larger SAP particle sizes, as confirmed by literature (Snoeck et al., 2014) and through the previous ultrasonic experiments. In contrast to the mortar specimens, an almost identical variation in crack width was observed for all compositions during the first three days of curing. Afterwards, the healing trend slightly slowed down, but a continuous improvement could be noticed until 28 days of wet-dry curing. This difference between mortar and concrete, i.e. the fast crack filling during first three days within mortar and the more gradual reduction in crack width within concrete, is supported by the attenuation graphs in Fig. 6. A similar explanation could be given here, being that the presence of aggregates hinders the contact between water and reactants, while the available cross-section to be healed is smaller in concrete, compared to mortar. Therefore, there is a rapid filling in mortars that terminates upon consummation of the reactants, while a more continuous, but slower deposition of healing products is noticed for concrete.

Since the ultrasonic measurements and microscopic analysis both demonstrate the deposition of healing products, a correlation between the outcomes of these techniques would prove to be interesting. It should be mentioned, however, that the ultrasonic measurements provide information on a zone with a depth of a few mm below the surface, while microscopy assesses only the visible part of the crack on the surface. The depth of penetration of ultrasound can be roughly of the order of 20–25 mm, considering a wave velocity of 4000 m/s and the transducers' frequency of 150 kHz. In case of microscopy, two, respectively three, positions along the crack length were chosen for mortar and concrete, as these measurements only describe the crack width at discrete positions. A one-on-one correlation should therefore not be expected, but a distinct trend could be visible. In Fig. 10 (a), the longitudinal wave velocity is plotted with respect to the average crack width of the mortar specimens. The velocity shows a decreasing trend for larger crack widths, and this for all mixtures tested. In the intact state (having a crack width equal to 0 μm) longitudinal wave velocities above 3500 m/s were obtained. After cracking, indicated by the values around 150 μm, the velocity drops below 3000 m/s. As the samples are healing within wet-dry cycles, a noticeable increase of the velocity goes along with the reduction of the observed crack width on the surface. The attenuation vs. crack width, plotted in Fig. 10 (b), demonstrates a monotonic increase of attenuation with crack size. Before crack creation, the attenuation was limited to values below 0.25 dB/mm, while immediately after cracking the highest attenuation values were obtained, i.e. between 0.4 dB/mm and 0.5 dB/mm. The intermediate values designate the partial crack healing of all mortar specimens.

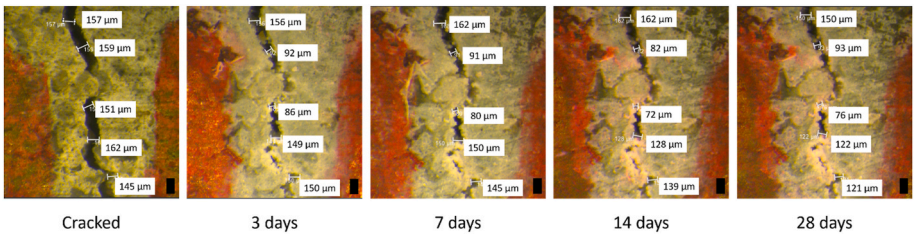

Fig. 8. Evolution of the crack width during wet-dry curing of a representative reference mortar specimen. The black rectangles in the lower right corners have a height of 200 µm.

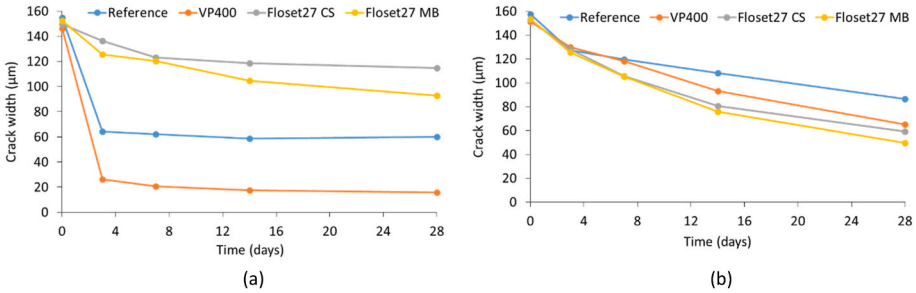

Fig. 9. Evolution of the crack width vs. time for (a) mortar and (b) concrete mixtures.

Table 3
Average crack width (µm) and standard deviation (µm) of mortar (n = 10) and concrete (n = 15) mixtures during wet-dry healing.

		Mortar	Concrete
Reference	Cracked	155 ± 9	158 ± 8
	3 days	64 ± 55	127 ± 6
	7 days	62 ± 56	119 ± 8
	14 days	59 ± 56	108 ± 6
	28 days	60 ± 56	86 ± 7
VP400	Cracked	146 ± 10	151 ± 7
	3 days	26 ± 34	130 ± 5
	7 days	21 ± 30	118 ± 7
	14 days	17 ± 30	93 ± 8
	28 days	16 ± 25	65 ± 7
Floset27 CS	Cracked	150 ± 7	153 ± 6
	3 days	136 ± 13	128 ± 5
	7 days	123 ± 15	106 ± 8
	14 days	119 ± 19	81 ± 7
	28 days	115 ± 22	59 ± 8
Floset27 MB	Cracked	152 ± 6	153 ± 8
	3 days	126 ± 25	126 ± 6
	7 days	120 ± 27	105 ± 6
	14 days	105 ± 31	76 ± 7
	28 days	93 ± 31	50 ± 7

Focusing on the concrete mixtures, similar trends between the crack width and the longitudinal wave velocity or attenuation were observed. Fig. 11 (a) shows the decreasing tendency of the wave velocity with increasing crack widths, while in Fig. 11 (b) a higher attenuation corresponds to a larger crack size. The linear fitting lines are given only indicatively, to demonstrate the positive or negative trends, while other higher order functions possibly provide better correlation coefficients.

As a summary, it should be mentioned that the exact reasoning behind the higher healing effectiveness of VP400 SAPs in mortar, in contrast to the increased restoration upon inclusion of Floset27 SAPs in concrete, is still under investigation. Further research is needed to clarify the mechanisms of SAP-induced self-healing within these distinct cementitious blends, as it is the first time that a direct comparison between the healing ability of SAP-holding mortar and concrete is presented. Nonetheless, the results above, comparing the ultrasonic parameters to the microscopic analysis, confirm the sensitivity of ultrasound to the deposition of healing products inside the crack. Whereas these cracks only account for a very small portion of the wave's propagation path between the sensors (150 µm or approximately 0.4% of the distance between the receivers), both the crack creation and its filling lead to distinct variations in the ultrasonic parameters. Moreover, the use of ultrasound allowed to distinguish between the healing ability of different SAPs, showing higher restoration of ultrasonic parameters in case of mixtures with improved crack closure, while at the same time enabling the assessment of a material with an increased amount of large scatterers (concrete vs. mortar).

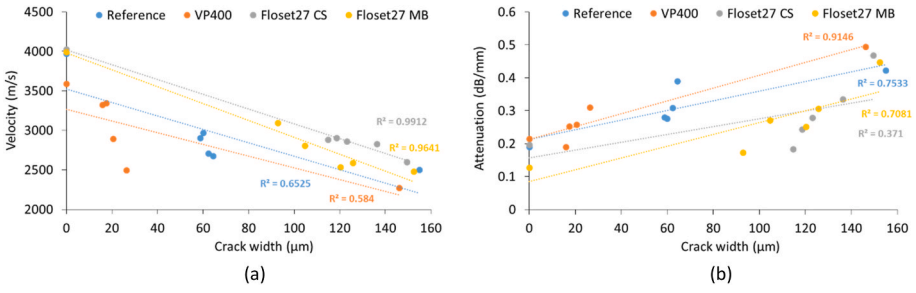

Fig. 10. (a) Longitudinal wave velocity and (b) attenuation vs. average crack width for mortar mixtures.

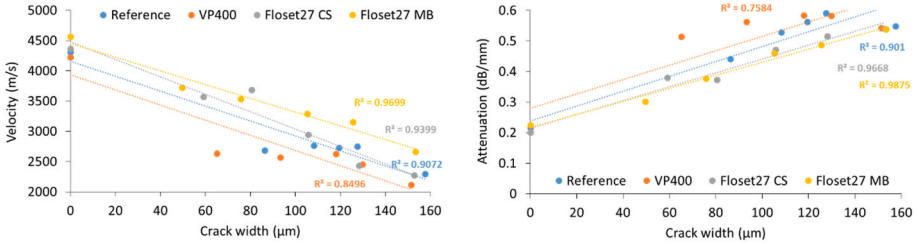

Fig. 11. (a) Longitudinal wave velocity and (b) attenuation vs. average crack width for concrete mixtures.

4. Summary and conclusion

In this study, the self-healing ability of four concrete mixtures and their equivalent mortar blends was investigated through ultrasonic surface wave measurements and microscopic analysis. The mixtures comprised a reference material without additives and three mixtures with different superabsorbent polymers. All specimens were cracked after 28 days of curing and wet-dry healing cycles were applied to promote the healing mechanism.

Concerning the ultrasonic measurements, the intact, cracked and healed stages of the cementitious blends were evaluated through the longitudinal wave velocity and the attenuation. In the uncracked state, velocities above 3500 m/s were measured for all mixes corresponding to high quality material. Subsequently, the crack creation was noticed by a strong reduction of the wave velocity and an increase in the attenuation for all materials tested. Upon the application of wet-dry curing cycles, a partial restoration was noticed over time for all specimens under study. Attenuation measurements consistently indicated a more intensive restoration for mortar during the first week, while concrete exhibited a more gradual and continuous trend until the final measurement of 28 days, being in accordance with the microscopy trends. Furthermore, the ultrasonic results demonstrated the difference in self-healing effectiveness between the various SAPs used, and their differential influence in the two material types. Specifically, the VP400 SAP showed the highest restoration within mortars, while Floset27 CS and Floset27 MB were most effective inside concrete samples.

Through microscopic analysis, the filling of the cracks at the surface was monitored. The results indicated partial filling of the cracks within all materials under study. Nonetheless, a difference in the self-healing capacity upon the inclusion of various SAPs was observed. A comparison between the average crack width and the ultrasonic parameters (longitudinal wave velocity and attenuation) confirmed a correlation between the deposition of healing products and the ultrasonic wave propagation. More specifically, a monotonic reduction of the longitudinal wave velocity with increasing crack width was obtained, while the attenuation increased for larger crack sizes.

It can be concluded that the adoption of ultrasonic surface wave measurements provides invaluable information on the self-healing evolution of cementitious blends. Thanks to its sensitivity down to the micro-scale, ultrasound allows to evaluate the healing ability of various superabsorbent polymers, enabling the selection of the ideal SAP to be included in a certain mixture to promote self-healing. The correlation between ultrasonic parameters and microscopic analysis supports the added value of ultrasound, revealing the closure of cracks in a fast, easily applicable manner compared to time-consuming microscopic analysis.

Declaration of competing interest

The authors declare that they have no known competing financial interests or personal relationships that could have appeared to influence the work reported in this paper.

Acknowledgements

The authors wish to thank the Vrije Universiteit Brussel (VUB) for the financial support through an OZR backup mandate (OZR3776). Also, we wish to express our gratitude to Mr. Guillaume Jeanson (SNF) and Dr. Alexander Assmann (BASF) for providing the SAPs under study.

References

Aggelis, D., Shiotani, T., Polyzos, D., 2009. Characterization of surface crack depth and repair evaluation using Rayleigh waves. Cement Concr. Compos. 31 (1), 77–83.
Ahn, E., Kim, H., Sim, S., Shin, S., Shin, M., 2017. Principles and applications of ultrasonic-based nondestructive methods for self-healing in cementitious materials. Materials 10 (3), 278.
Ahn, E., Kim, H., Park, B., Shin, M., 2021. Long-term autogenous healing and re-healing performance in concrete: evaluation using air-coupled surface-wave method. Construct. Build. Mater. 307, 124939.
Antonaci, P., Bruno, C., Gliozzi, A., Scalerandi, M., 2010. Monitoring evolution of compressive damage in concrete with linear and nonlinear ultrasonic methods. Cement Concr. Res. 40 (7), 1106–1113.
Belgisch instituut voor normalisatie (BIN), 1999. Methods of Test for Mortar Masonry - Part 3: Determination of Consistence of Fresh Mortar *(by flow table)*.
Chaix, J.-F., Garnier, V., Corneloup, G., 2006. Ultrasonic wave propagation in heterogeneous solid media: theoretical analysis and experimental validation. Ultrasonics 44 (2), 200–210.
Craeye, B., Geirnaert, M., De Schutter, M., 2011. Super absorbing polymers as an internal curing agent for mitigation of early-age cracking of high-performance concrete bridge decks. Construct. Build. Mater. 25 (1), 1–13.
De Belie, N., Grosse, C., Kurz, J., Reinhardt, H., 2005. Ultrasound monitoring of the influence of different accelerating admixtures and cement types for shotcrete on setting and hardening behaviour. Cement Concr. Res. 35, 2087–2094.
De Meyst, L., Mannekens, E., Van Tittelboom, K., De Belie, N., 2021. The influence of superabsorbent polymers (SAPs) on autogenous shrinkage in cement paste, mortar and concrete. Construct. Build. Mater. 286, 122948.
Fan, S., Li, S., 2014. X-ray computed microtomography of three-dimensional microcracks and self-healing in engineered cementitious composites. Smart Mater. Struct. 24 (1), 015021.
Gruyaert, E., Debbaut, B., Snoeck, D., Diaz, P., Arizo, A., Tziviloglou, E., Schlangen, E., De Belie, N., 2016. Self-healing mortar with pH-sensitive superabsorbent polymers: testing of the sealing efficiency by water flow tests. Smart Mater. Struct. 25 (8), 084007.
Haach, V., Marrara Juliani, L., Ravanini Da Roz, M., 2015. Ultrasonic evaluation of mechanical properties of concretes produced with high early strength cement. Construct. Build. Mater. 96, 1–10.
Hasholt, M., Jespersen, M., Jensen, O., 2010. Mechanical properties of concrete with SAP part I: development of compressive strength. In: International RILEM Conference on Use of Superabsorbent Polymers and Other New Additives in Concrete. Lyngby, Denmark.
Hossain, M., Sultana, R., Patwary, M., Khunga, N., Sharma, P., Shaker, S., 2022. Self-healing concrete for sustainable buildings. A review. Environ. Chem. Lett. 20, 1265–1273.
Kanellopoulou, I., Kartsonakis, I., Charitidis, C., 2021. The effect of superabsorbent polymers on the microstructure and self-healing properties of cementitious-based composite materials. Appl. Sci. 11 (2), 700.
Kaplan, M., 1959. The effects of age and water/cement ratio upon the relation between ultrasonic pulse velocity and compressive strength of concrete. Mag. Concr. Res. 11 (32), 85–92.
Lefever, G., Snoeck, D., Aggelis, D., De Belie, N., Van Vlierberghe, S., Van Hemelrijck, D., 2020a. Evaluation of the self-healing ability of mortar mixtures containing superabsorbent polymers and nanosilica. Materials 13 (2), 380.
Lefever, G., Aggelis, D., De Belie, N., Raes, M., Hauffman, T., Van Hemelrijck, D., Snoeck, D., 2020b. The influence of superabsorbent polymers and nanosilica on the hydration process and microstructure of cementitious mixtures. Materials 13 (22), 5194.

Lefever, G., Snoeck, D., De Belie, N., Van Vlierberghe, S., Van Hemelrijck, D., Aggelis, D., 2020c. The contribution of elastic wave NDT to the characterization of modern cementitious media. Sensors 20 (10), 2959.
Lefever, G., Snoeck, D., De Belie, N., Van Hemelrijck, D., Aggelis, D., 2021. Elastic wave monitoring of cementitious mixtures including internal curing mechanisms. Sensors 21, 2463.
Lefever, G., Van Hemelrijck, D., Snoeck, D., Aggelis, D., 2022. Self-healing assessment of cementitious mortars through ultrasonic monitoring. Cement Concr. Compos. 133, 104683.
Naik, T., Malhotra, V., Popovics, J., 2003. The ultrasonic pulse velocity method. In: Handbook on Nondestructive Testing of Concrete, second ed. (Chapter 8).
Pelto, J., Leivo, M., Gruyaert, E., Debbaut, B., Snoeck, D., De Belie, N., 2017. Application of encapsulated superabsorbent polymers in cementitious materials for stimulated autogenous healing. Smart Mater. Struct. 26, 105043.
Popovics, S., 2001. Analysis of the concrete strength versus ultrasonic pulse velocity relationship. Mater. Eval. 59 (2), 123–130.
Qian, S., Zhou, J., de Rooij, M., Schlangen, E., Ye, G., van Breugel, K., 2009. Self-healing behavior of strain hardening cementitious composites incorporating local waste materials. Cement Concr. Compos. 31 (9), 613–621.
Schröfl, C., Erk, K., Siriwatwechakul, W., Wyrzykowski, M., Snoeck, D., 2022. Recent progress in superabsorbent polymers for concrete. Cement Concr. Res. 151, 106648.
Selleck, S., Landis, E., Peterson, M., Shah, S., Achenbach, J., 1998. Ultrasonic investigation of concrete with distributed damage. ACI Mater. J. 95, 27–36.
Snoeck, D., De Belie, N., 2015. Repeated autogenous healing in strain-hardening cementitious composites by using superabsorbent polymers. J. Mater. Civ. Eng. 28 (1), 04015086.
Snoeck, D., De Belie, N., 2019. Autogenous healing in strain-hardening cementitious materials with and without superabsorbent polymers: an 8-year study. Frontiers in Materials 6 (48), 1–12.
Snoeck, D., Van Tittelboom, K., Steuperaert, S., Dubruel, P., De Belie, N., 2014. Self-healing cementitious materials by the combination of microfibres and superabsorbent polymers. J. Intell. Mater. Syst. Struct. 25 (1), 13–24.
Suleiman, A., Nelson, A., Nehdi, M., 2019. Visualization and quantification of crack self-healing in cement-based materials incorporating different minerals. Cement Concr. Compos. 103, 49–58.
Tsangouri, E., Lelon, J., Minnebo, P., Asaue, H., Shiotani, T., Van Tittelboom, K., De Belie, N., Aggelis, D., Van Hemelrijck, D., 2019. Feasibility study on real-scale, self-healing concrete slab by developing a smart capsules network and assessed by a plethora of advanced monitoring techniques. Construct. Build. Mater. 228, 116780.
Van Mullem, T., Gruyaert, E., Debbaut, B., Caspeele, R., De Belie, N., 2019. Novel active crack width control technique to reduce the variation on water permeability results for self-healing concrete. Construct. Build. Mater. 203, 541–551.
Van Tittelboom, K., De Belie, N., 2013. Self-healing in cementitious materials - a review. Materials 6, 2182–2217.
Wang, J., Soens, H., Verstraete, W., De Belie, N., 2014. Self-healing concrete by use of microencapsulated bacterial spores. Cement Concr. Res. 56, 139–152.
Wehbe, Y., Ghahremaninezhad, A., 2017. Combined effect of shrinkage reducing admixtures (SRA) and superabsorbent polymers (SAP) on the autogenous shrinkage, hydration and properties of cementitious materials. Construct. Build. Mater. 138, 151162.